### Title

Successive removal of E. coli and a mixture of Pb2+ and malachite green from water via magnetic iron oxide/phosphate nanocomposites




### Authors

Zhang, Fan
Wu, Zhaozhao
Huang, Yuxiong
et al.



### Publication Date

2019-10-01

### DOI

10.1016/j.colsurfa.2019.123598

Peer reviewed

Colloids and Surfaces A 578 (2019) 123598

Contents lists available at ScienceDirect

Colloids and Surfaces A

journal homepage: www.elsevier.com/locate/colsurfa

# Successive removal of *E. coli* and a mixture of $Pb^{2+}$ and malachite green from water via magnetic iron oxide/phosphate nanocomposites

Fan Zhang[a,*], Zhaozhao Wu[a], Yuxiong Huang[b,c], Arturo A. Keller[c]

[a] College of Science, Nanjing Agricultural University, Nanjing 210095, PR China
[b] Shenzhen Environmental Science and New Energy Technology Engineering Laboratory, Tsinghua-Berkeley Shenzhen Institute, Shenzhen 518055, PR China
[c] Bren School of Environmental Science and Management, University of California, Santa Barbara, CA, 93106, USA

## GRAPHICAL ABSTRACT

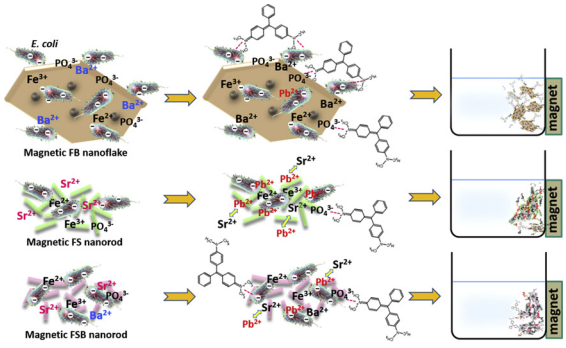


## ARTICLE INFO

*Keywords:*
Magnetic phosphate nano-composites
Successive remediation
Multiple contaminants
Disinfection

## ABSTRACT

Three magnetic iron oxide/phosphate nanocomposites, $Fe_3O_4/Ba_3(PO_4)_2$, $Fe_3O_4/Sr_5(PO_4)_3(OH)$, and $Fe_3O_4/Sr_{5x}Ba_{3x}(PO_4)_3(OH)$ (denominated FB, FS, and FSB, respectively) were prepared by one-pot hydrothermal method. They exhibited a removal efficiency of 96%, 86%, and 91% for *Escherichia coli* (*E. coli*) of $5 \times 10^8$ CFU/mL within 30 min, respectively. After bacterial removal, the recovered nano-composites by a magnet were re-used to treat a mixed solution of $Pb^{2+}$ and malachite green (MG). The loaded *E. coli* on the surface of the nanocomposites is beneficial to the subsequent removal of positively charged $Pb^{2+}$ and MG. On the other hand, the MG in the mixture can contribute substantially to the disinfection of the recovered nanocomposites. These nano-composites are sustainable materials for the successive removal of *E. coli* and mixed cationic pollutants from water. Removal process by these nano-composites possesses a synergistic effect, leading to more effective water treatment.

## 1. Introduction

Water contamination with multiple contaminants, such as bacteria, organic dyes, and heavy metal ions, poses a serious threat to human health [1–3]. Thus, there is an urgent demand for the development of better techniques for purifying water by simultaneously removing multiple contaminants. *Escherichia coli* (*E. coli*) is commonly used as an indicator of fecal contamination to evaluate and monitor water quality [4]. And $Pb^{2+}$ and malachite green (MG) are easily found in wastewater due to their common usage in industry [5]. Numerous materials

* Corresponding author.
*E-mail address:* zhangfan0128@njau.edu.cn (F. Zhang).

https://doi.org/10.1016/j.colsurfa.2019.123598
Received 1 April 2019; Received in revised form 21 June 2019; Accepted 21 June 2019
Available online 28 June 2019
0927-7757/ 

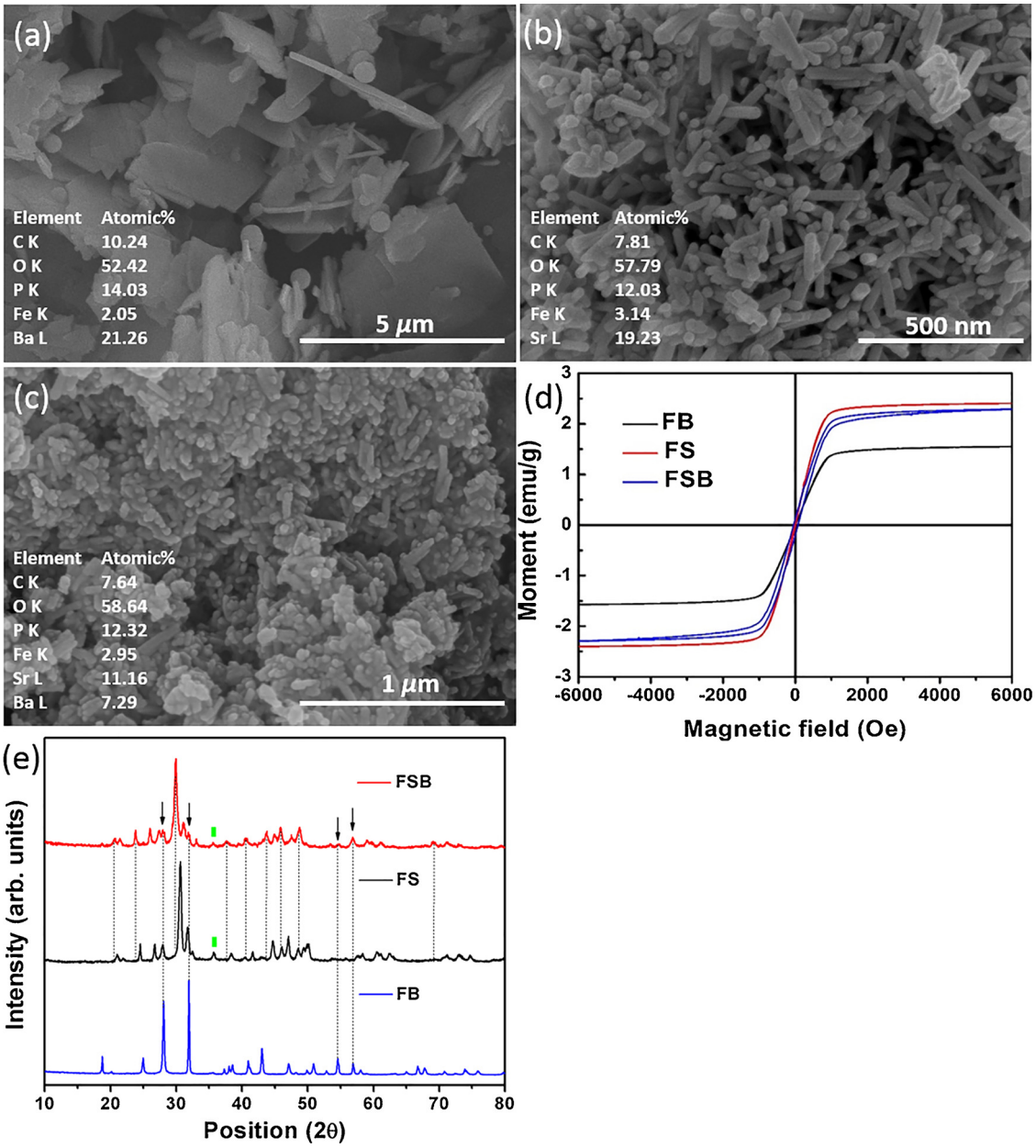


**Fig. 1.** SEM image of (a) FB with a scale bar of 5 μm, (b) FS with a scale bar of 500 nm, (c) FSB with a scale bar of 1 μm, (d) magnetic hysteresis loops, and (e) XRD patterns of FB, FS, and FSB.

have been developed for removing these pollutants from [6–8]. However, many materials reported in previous works were limited to be used for removing one type of pollutants [9–11] and it is still a major challenge to effectively remove several pollutants from wastewater by using one simple material [12] which will decrease the cost of materials. Especially, there is a need for nanomaterials that can successively remove different types of pollutants. This could happen with mixed wastes from sewage, electroplating and textile discharges [13].

It is well known that $Fe_3O_4$-containing adsorbents present several advantages, such as convenient functionalization with other materials and ease of separation from suspension via a magnetic field. Easy removal avoids secondary pollution and reduces operating costs in wastewater treatment [9]. $Fe_3O_4$-containing materials are usually structured with different components, to incorporate multiple properties in the same nanomaterial [13]. Only a limited number of magnetic nanocomposites have been reported for simultaneously removing bacteria and other kinds of pollutants [14–26]. For example, magnetic graphene was used to reduce heavy metals and bacteria in water [15]; silver-iron oxide nanoparticles on the surface of fly ash were employed to remove bacteria and $Pb^{2+}$ [25]; a magnetic chitosan-graphene oxide composite was developed for anti-microbial and dye removal [26]. However, the nanomaterials in most previous studies were used to address one kind of pollutant (i.e. bacteria, dyes or metal ions) in each treatment with a limited initial bacterial concentration ($C_0 = 10^5$-$10^7$ CFU/mL) [20–22]. Studies on the successive removal of several pollutant types and understanding the interaction mechanisms between several pollutants with a multi-functional magnetic material are still rare.

Magnetic iron oxide/phosphate nanocomposites were reported to be effective and recyclable adsorbents for *E. coli*, organic dyes or $Pb^{2+}$ [27,28]. However, the successive removal of multiple contaminants from water by these functional nanocomposites has not been reported. It should be noted that these magnetic iron oxide/phosphate nanocomposites possessed a negatively charged surface after *E. coli* removal [4], which may be beneficial to subsequent removal of positive

**Table 1**
Comparisons of the initial concentration of *E. coli* ($C_0$), material dosage, and removal efficiency and capacity between the magnetic iron/phosphate nanocomposites in this work and other magnetic composites in recent reports.

| Material | $C_0$ (CFU/mL) | Dosage (mg/mL) | Removal efficiency | Capacity (CFU/mg) | Reference |
|---|---|---|---|---|---|
| Ag-$Fe_3O_4$/g-$C_3N_4$ nanocomposite | $10^7$ | 0.4 | 99% | $2.5 \times 10^7$ | [31] |
| Amino acid modified magnetic nanoparticles | $1.5 \times 10^7$ | 0.8 | 97% | $1.82 \times 10^7$ | [32] |
| $Fe_3O_4$@CTAB | $1.5 \times 10^7$ | 0.5 | 99% | $2.97 \times 10^7$ | [33] |
| $Fe_3O_4$-$SiO_2$-$NH_2$ nanoparticles | $10^2$ | 3 | 98.2% | 32.7 | [34] |
| $Fe_3O_4$-ZnO nanocomposite | $2.1 \times 10^7$ | 2 | 99.97% | $1.05 \times 10^7$ | [35] |
| Magnetic graphene composite | $10^6$ | 0.25 | 93.09% | $3.72 \times 10^6$ | [36] |
| Bacteriophage-based nanoprobes | $10^2$-$10^7$ | 1.8 | 92% | $5.1 \times 10^6$ | [37] |
| Anti-fimbrial modified magnetic reduced grapheme oxide nanoheaters | $10^9$ | 500 | 62% | $1.24 \times 10^6$ | [38] |
| Ag-$CoFe_2O_4$-GO nanoparticle | $10^5$ | 0.05 | 98.9% | $1.98 \times 10^6$ | [21] |
| Magnetic chitosan-graphene oxide composite | $10^5$-$10^6$ | 0.2 | 99% | $4.95 \times 10^6$ | [26] |
| Immunomagnetic particles | $10^2$-$10^5$ | 100 | 90% | 900 | [39] |
| FB | $5 \times 10^8$ | 2 | 97% | $2.43 \times 10^8$ | This work |
| FSB | $5 \times 10^8$ | 2 | 91% | $2.28 \times 10^8$ | This work |
| FS | $5 \times 10^8$ | 2 | 79% | $1.98 \times 10^8$ | This work |

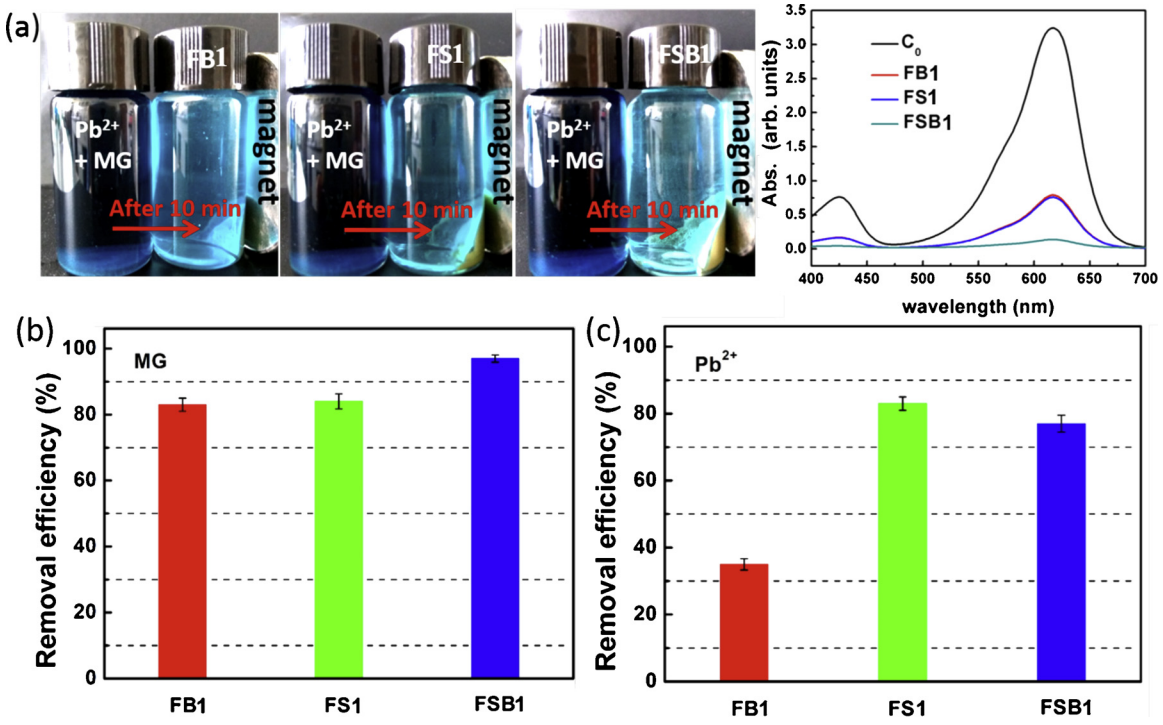


**Fig. 2.** (a) Visible color changes and UV spectrum of MG, and removal efficiency of (b) MG and (c) $Pb^{2+}$ from a mixture by the reclaimed FB1, FS1, and FSB1 after bacterial removal (0.06 g reclaimed nanocomposites, $C_0(Pb^{2+}) = C_0(MG) = 100$ mg/L, 50 mL, 25 °C, pH 4.8, 10 min).

pollutant ions (e.g. $Pb^{2+}$ and MG). To remove several pollutants from wastewater by using one simple material will decrease the cost of materials in the practical application.

In this study, we evaluated the removal and disinfection performance of $Fe_3O_4/Ba_3(PO_4)_2$, $Fe_3O_4/Sr_5(PO_4)_3(OH)$, and $Fe_3O_4/Sr_{5x}Ba_{3x}(PO_4)_3(OH)$ (denominated FB, FS, and FSB, respectively) for heavily *E. coli* contaminated water, and the subsequent removal of cations (e.g. $Pb^{2+}$ and MG) from a separate solution, after the *E. coli*-loaded nanocomposites were recovered using a magnet. The subsequent reuse of the nanocomposites results in a more sustainable use and multifunctional water treatment by these materials. This detailed study provides an insight into the mechanisms employed in a highly effective multi-contaminant water treatment.

## 2. Materials and methods

### 2.1. Synthesis of materials

The $Fe_3O_4$ spherical nano-crystalline (5–10 nm) cluster was prepared by a simple solvothermal method, as reported in our previous work [9]. Briefly, the FB or FS or FSB composites were prepared by one-pot hydrothermal method: 1.96 g barium nitrate or 1.59 g strontium nitrate or 0.98 g barium nitrate, 0.79 g strontium nitrate, 0.06 g $Fe_3O_4$ spherical clusters, and 0.01 g cetyltrimethyl ammonium bromide were added into 40 mL of deionized (DI) water under stirring to form Solution 1. Solution 2 was prepared by adding 0.82 g sodium phosphate into 10 mL of DI water at 40 °C with continuous stirring for 30 min. Solution 2 was slowly poured into Solution 1 with continuous stirring for 30 min. The mixed solution was then transferred into a 100 mL Teflon bottle, held in a stainless steel autoclave reactor, sealed, and maintained at 180 °C for 8 h. As the autoclave cooled to 25 °C, the obtained powder

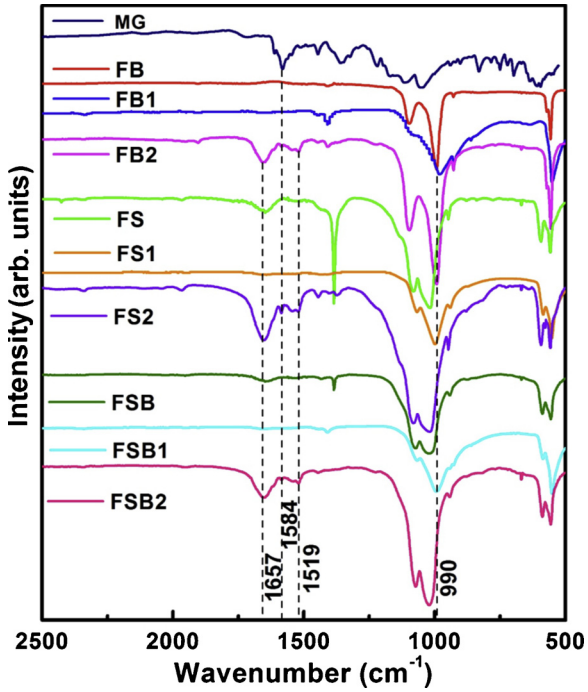


**Fig. 3.** FT-IR spectra of MG; pristine FB, FS, and FSB; FB1, FS1, and FSB1 after bacterial removal; FB2, FS2, and FSB2 after successive removal of *E. coli* and a mixture of $Pb^{2+}$ and MG.

was washed by DI water and ethanol for five times each. Finally, samples were dried at 60 °C for 4 h, and the yield was ~ 1.3 g with a yield ratio of ~85% at a material's cost of ~ $0.08/g.

### 2.2. Batch experiments

Generally, the removal efficiency of *E. coli* by FB, FS, or FSB was performed by adding 0.1 g material into 50 mL of *E. coli* suspension ($5 \times 10^8$ CFU/mL) at 25 °C and pH 6.0 under mechanical stirring at 250 rpm for 30 min. To investigate the influence of pH, temperature and dosage of material, the studies were done at different pH values (5, 6, 7, 8, 9), temperatures (20, 25, 30, 35, 40 °C) and dosage of material (0.02 g, 0.05 g, 0.08 g, 0.10 g, 0.15 g), respectively. The kinetic study was conducted at different interaction time (10, 20, 30, 40, 50 min). The removal capacity of FB, FS, or FSB was evaluated by changing the initial concentration of *E. coli* from $2.5 \times 10^8$ to $12.5 \times 10^8$ CFU/mL. Once bacterial removal reached a stable level, the bacteria-loaded FB/FS/FSB (denominated FB1, FS1, and FSB1) were separated from solutions by a small neodymium magnet (diameter of 50 mm, thickness of 5 mm). The residual concentration of the *E. coli* suspension was confirmed via $OD_{600}$.

The chemical structure of MG is shown in Fig. S1. Since no obvious interferences were observed in the UV spectrum of MG and $Pb^{2+}$ (Fig. S2), a mixed solution of $Pb^{2+}$ and MG with initial concentrations at 100 mg/L (each) was prepared in DI water, adjusting pH to 4.8 by 0.01 M $HNO_3$ to avoid the hydrolysis or precipitation of $Pb^{2+}$ [29]. The reclaimed FB1, FS1, and FSB1 were then employed to purify 50 mL of the mixed solutions containing both $Pb^{2+}$ (initial concentration = $C_0$ = 100 mg/L) and MG ($C_0$ = 100 mg/L) to evaluate the removal capacity of these reused materials in a typical complicated wastewater treatment. After removal, 1 mL of the suspension was sampled, then filtered with a 0.45 μm membrane, diluted, following by analysis using inductively coupled plasma atomic emission spectrometry (ICP-AES, Optima 2100, PerkinElmer, USA) and UV spectrophotometer (Shimadzu, model UV1700, Japan) to determine the concentration of $Pb^{2+}$ and MG, respectively.

All experiments were performed in three replicates and the average results were reported. The final materials after successive removal of *E. coli* suspension and mixed solution of $Pb^{2+}$ and MG (denominated as FB2, FS2, and FSB2) were further analyzed. Detailed preparation of *E. coli* suspension, fluorescent-based cell live/dead test and dilution plate count method, and characterization are described in supporting information.

## 3. Results and discussion

### 3.1. Characterization of materials

SEM images and EDS results of FB, FS and FSB are shown in Fig. 1a-c. FB exhibited a flake-like nanostructure with a thickness of ~100 nm and a length of 2–4 μm, blended with some $Fe_3O_4$ spherical particles with a mean particle size of ~500 nm. With a bigger size than *E. coli* (700 nm–1.2 μm) [4], the FB flakes provide a valuable surface for bacterial adhesion [4]. FS and FSB are all nanorods with a width of ~40 nm; FS (~200 nm) is longer than FSB (~100 nm). Hence, FSB with a smaller size showed aggregation with less hole between these nanorods. Notably, FS and FSB with a smaller size than *E. coli* may adhere onto the surface of *E. coli*, similar to $Fe_3O_4$ spherical particles [4]. ESD results demonstrated that the main composition of these nanocomposites are metal (Sr and/or Ba) phosphate with a lower concentration of 2.05, 3.14, and 2.95 atomic% for Fe in FB, FS, and FSB, respectively. However, FB, FS, and FSB have a saturated magnetization value of 1.6, 2.4, and 2.3 emu/g, respectively (Fig. 1d), which allows the magnetic separation of these materials by a magnet from water. From the XRD patterns (Fig. 1e), all the main characteristic peaks were attributed to the diffraction of crystal planes of $Ba_3(PO_4)_2$ (rhombohedral crystal structure), $Sr_5(PO_4)_3(OH)$ (hexagonal crystal structure), and $Sr_{5x}Ba_{3x}(PO_4)_3(OH)$ (mainly hexagonal crystal structure), respectively, agreeing with the EDS results. The peak at 30.3° (marked green) and some small peaks (marked with arrows) were assigned to diffraction from the (220) crystal plane of $Fe_3O_4$ [30] and corresponding crystal planes of $Ba_3(PO_4)_2$ [4], respectively.

The BET surface areas of FB, FS, and FSB are 12.4, 49.3, and 55.8 $m^2/g$, respectively. The Barrett-Joyner-Halenda (BJH) adsorption cumulative volume of pores for FB, FS, and FSB is 0.02, 0.12, and 0.14 $cm^3/g$ with an average pore width (4 V/A) of 25.5, 40.5, and 46.7 Å, respectively. The low leaching of phosphate (0.09 mg/L) and metal (5.7–9.2 μg/L of Fe, 0–11.4 μg/L of Sr, 3.9–12.8 μg/L of Ba) in solutions detected by ICP-AES demonstrated the chemical stability of FB, FS, and FSB in water (pH 6).

### 3.2. Removal of E. coli

After exploring a range of conditions (Fig. S3), 35 °C, 30 min, and a dosage of 0.10 g/50 mL were considered most suitable for treating *E. coli* suspensions of $5 \times 10^8$ CFU/mL by FB, FS, and FSB. The three nanocomposites studied here were capable of working with a much higher bacterial load capacity ($(1.98–2.43) \times 10^8$ CFU/mg) than other similar magnetic materials (Table 1) and maintained high removal efficiencies (> 80%) even after five cycles (Fig. S3g). In addition, the recyclable magnetic materials in this work are inorganic and can be easily prepared by a simple one-pot hydrothermal method, suggesting that they are economic and environmentally friendly. These confirm that FB, FS, and FSB are efficient and promising materials for the removal of *E. coli* from contaminated waters. In addition, less than 20% of the bacteria loaded on FB1 and FSB1 leach back to the wash water even after the nanocomposites have been washed four times (Fig. S5), which can avoid secondary pollution to the water system. Since the FS nanorods had the smallest surface charge (13.7, 7.6, and 4.9 mV for FB, FSB, and FS, respectively), FS exhibited the lowest removal capacity of *E. coli* among the three nanomaterials (Table S1). FS had the weakest electrostatic interaction with negatively charged *E. coli* [15], which also

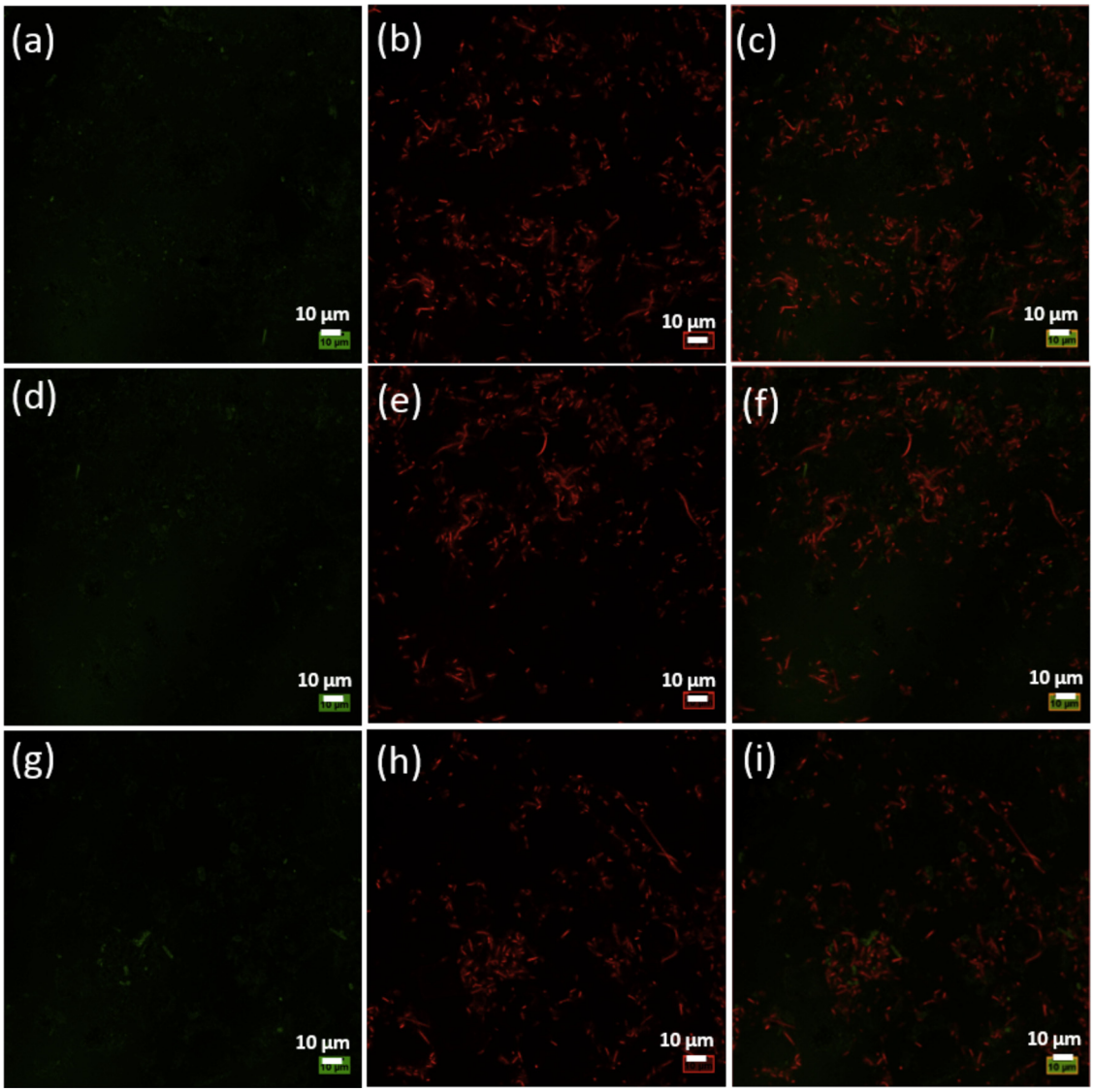


**Fig. 4.** Confocal fluorescent images of live and dead bacterial cells attached onto (a–c) FB2, (d–f) FS2, and (g–i) FSB2. (c, f, i) Overlying images of *E. coli* stained with SYTO9 (green) and PI (red). (For interpretation of the references to colour in this figure legend, the reader is referred to the web version of this article).

led to more bacteria being washed off and less bacteria remaining on FS (Fig. S5).

### 3.3. Simultaneous removal of $Pb^{2+}$ and MG after bacterial removal

Instead of washing off the *E. coli* loaded onto the nanocomposites, they can be used to remove metal ions and positively charged organic molecules based on two factors: (1) the change of surface charge of FB1, FSB1, and FS1 from positive to negative due to the presence of *E. coli* is beneficial for attracting positive ions through electrostatic interactions; (2) pure *E. coli* cells have a removal efficiency of 61% for $Pb^{2+}$ and 68% for MG (Fig. S6), thus their presence on the nanocomposites should promote removal of these cations.

Since pure MG solutions or the mixed solution of $Pb^{2+}$ and MG may affect the biological activity of *E. coli* (Fig. S7), we employed the reclaimed FB1, FS1, and FSB1 (about 0.06 g) to treat 50 mL of a mixed solution containing $Pb^{2+}$ and MG. All three types of reclaimed nanocomposites showed effective removal of MG within 10 min as the diminishment of green color and the decreased of absorbance under UV were observed in Fig. 2a. For the removal of MG from a mixed solution (Fig. 2b), FSB1 exhibited the highest removal efficiency with a calculated capacity of 80.8 mg/g, which is higher than that of the reclaimed FS1 (70.5 mg/g), FB1 (68.3 mg/g), and some other materials [23,40–42]. Since FSB1 possessed the most negative zeta potential (-20.4 mV) after it was loaded with bacteria, the electrostatic attraction is most beneficial to attach MG to the surface of FSB1. Furthermore, FSB1 has a more negative charge and a larger surface area than FB1 and FS1 after bacterial removal, which provides more binding sites for FSB1 to remove dye molecules through several interactions: (1) electrostatic attraction between negatively charged groups of FSB1 and the positive $= N^+(CH_3)_2$ group of MG; (2) hydrogen bonding between oxygen-containing groups of FSB1 and positively charged hydrogen in MG; and (3) Lewis acid-base interactions between Ba/Sr sites in FSB and $-N^+(CH_3)_2$ in MG.

As shown in Fig. 2c, FS1 showed the highest $Pb^{2+}$ removal efficiency (84%), while FB1 exhibited the lowest $Pb^{2+}$ removal efficiency (34%) due to the least number of effective sites for ion-exchange between $Sr^{2+}$ and $Pb^{2+}$ [43] after being covered by bacteria. The calculated removal capacities of $Pb^{2+}$ by FS1 and FSB1 are 70 mg/g and 64.2 mg/g, respectively, which are still higher than some previous studies with other materials [15,21,22]. FS1 showed a relatively higher removal efficiency of $Pb^{2+}$ than FSB1, which may be attributed to more $Sr^{2+}$ sites in FS for $Pb^{2+}$ (Fig. 1) and less bacteria covering the surface of FS1.

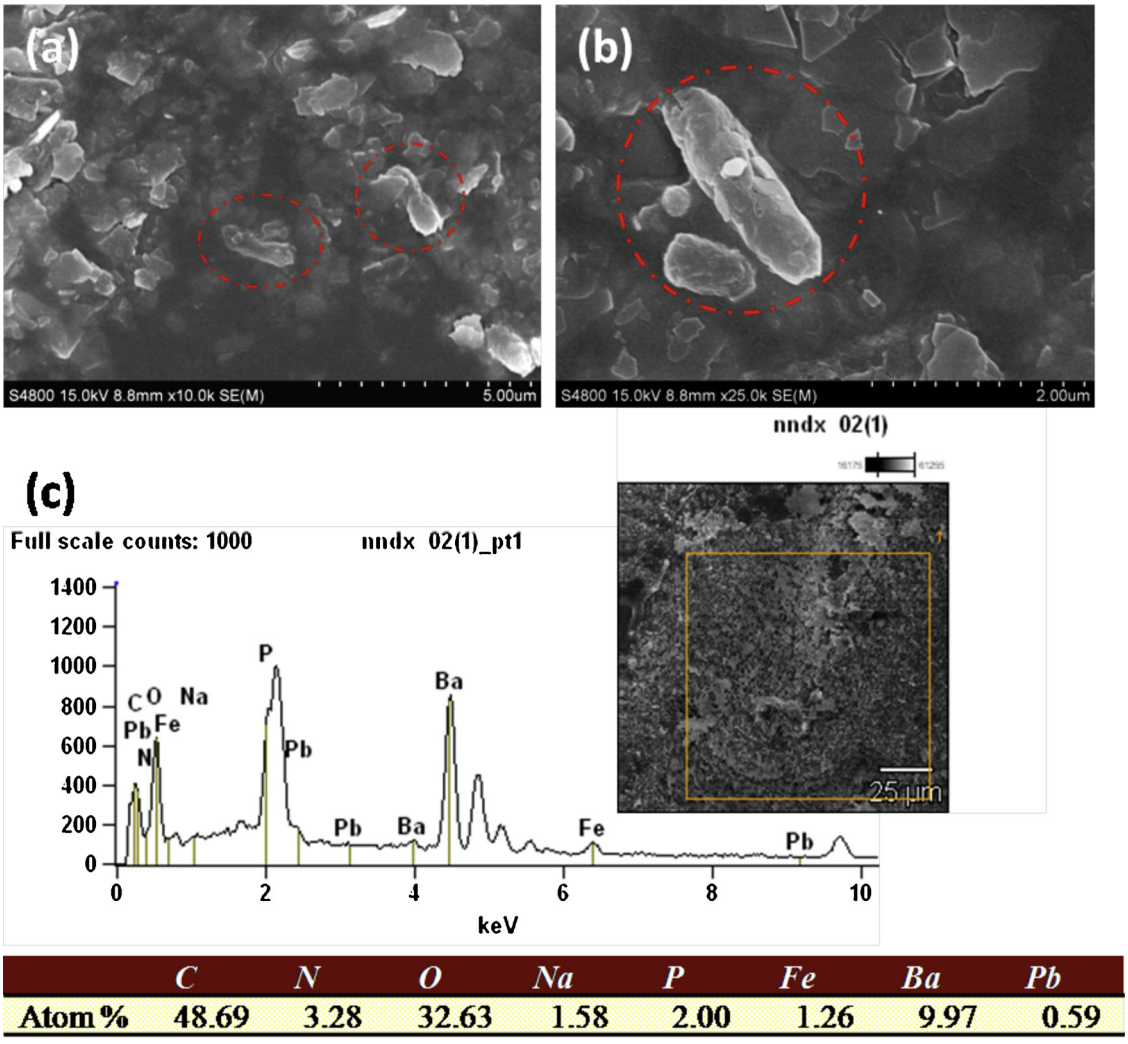


| | C | N | O | Na | P | Fe | Ba | Pb |
|---|---|---|---|---|---|---|---|---|
| Atom % | 48.69 | 3.28 | 32.63 | 1.58 | 2.00 | 1.26 | 9.97 | 0.59 |

**Fig. 5.** SEM of FB2 with a magnification of (a) 10.0 k and (b) 25.0 k; and (c) EDS results ($C_0$(*E. coli*) = 5 × $10^8$ CFU/mL, 35 °C, pH 6, 30 min; $C_0(Pb^{2+})$ = 100 mg/L, $C_0$(MG) = 100 mg/L, 25 °C, pH 4.8, 30 min).

Compared to the individual removal of $Pb^{2+}$ or MG by pristine FB, FS, and FSB (Fig. S8a and b), the removal efficiency for simultaneous removal of $Pb^{2+}$ and MG from a mixture decreased (Fig. S8c and d), indicating some competitive sorption between $Pb^{2+}$ and MG [14]. The removal efficiency of $Pb^{2+}$ by FB1 from the mixture (Fig. 2c) increased in comparison with that by FB (Fig. S8d). It results from the fact that the removal efficiency of $Pb^{2+}$ by *E. coli* was 61% (Fig. S6), which is higher than that of FB (Fig. S8b). Similarly, the removal efficiency of MG from mixed solution by FS1 and FSB1 (Fig. 2b) increased compared to that of pristine FS and FSB (Fig. S8c) which can be ascribed to the additional interactions between MG and loaded *E. coli* [44].

### 3.4. Mechanism of multifunctional removal

The spectra in Fig. 3 for all the magnetic materials display a broad band at 580 $cm^{-1}$, which is believed to be associated with the stretching vibrations of the tetrahedral groups ($Fe^{3+}$–$O^{2-}$) for $Fe_3O_4$ [45]. Compared to pristine FB, FS, and FSB, a wide peak was observed at 990 $cm^{-1}$ in FB1, FS1, and FSB1 (Fig. 3). This can correspond to the O—P—O vibrations of DNA of *E. coli* [46] which overlapped the stretching vibration peak of $PO_4^{3-}$ groups in the nanocomposites near this region [47]. After simultaneous removal of $Pb^{2+}$ and MG, the width of peaks in the region of 910-1200 $cm^{-1}$ increased for FB2, FS2, and FSB2 compared with the pristine materials. This can be assigned to the overlapping bands resulting from an increase in the number of phospholipids or phosphorylated proteins on the phosphate investigated [48]. This implies that the cell structure of *E. coli* was damaged by the nanocomposites and the inner cell contents were released [36,38]. The new peak at 1584 $cm^{-1}$ found in FB2, FS2, and FSB2 can be assigned to the C=N stretch mode [49], confirming the presence of MG in the final materials. The appearance of strong bands at frequencies of 1657 $cm^{-1}$ (C=O, amide I) and 1519 $cm^{-1}$ (ring vibration, Tyr) indicates the presence of protein in the solid state [50,51] from the loaded *E. coli* on the nanocomposites.

The XRD patterns of the final FB2, FS2, and FSB2 after multicomponent treatment are shown in Fig. S9. The main peaks and crystallographic structure of FB, FS, and FSB before and after treatment show no obvious change, implying that these materials are stable after multicomponent treatment. Notably, the peaks at around 31° and 25° for all the materials (marked arrows) are higher after treatment. They were assigned to the corresponding peaks of $PbHPO_4$ and $Pb_5(PO_4)_3(OH)$ [43], suggesting the immobilization of $Pb^{2+}$ in the lattice of FB2, FS2, and FSB2. In addition, according to the ICP-AES results (pH 4–6), 1.63%–4.27% of the loaded $Pb^{2+}$ and MG were leached from the reclaimed materials into solutions in the treatment process, which further implied the weak risk of second pollution to the water system by these materials.

Fluorescent-based cell tests of live and dead bacterial cells after the first bacterial removal and then simultaneous removal of $Pb^{2+}$ and MG were conducted (Fig. 4) to evaluate whether the adsorbed cells were

effectively inactivated. The strong red fluorescence intensity region in Fig. 4 indicates that around 99%, 99%, and 97% of the bacteria adhered to FB2, FS2, and FSB2 were dead [21], suggesting irreversibly damaged cell membranes or mass cell death [36] during the treatment. It should be noted that only around 30% of cells loaded on FB1, FS1, and FSB1 were dead before exposing them to the mixed solution (Fig. S10). This may result from irreversible cell structural damage and oxidation sterilization by these materials [4]. Additionally, $Pb^{2+}$ solution showed no noticeable disinfection effect (Fig. S7a-i). However, pure MG solution and mixed solution of $Pb^{2+}$ and MG were strong disinfectants under the same conditions (Fig. S7j-o). This implies that MG plays a significant role in the chemical disinfection process after physical cell damage and oxidation sterilization by the nanocomposites [4].

As shown in Fig. 5a and b, the treated *E. coli* cells were observed in the final FB2 after successive removal of *E. coli* and mixture of $Pb^{2+}$ and MG. However, the cell structure was seriously damaged and large cavities were seen on the surface of the cell membranes. Furthermore, the detection of Pb via EDS (Fig. 5c) and the color change of the materials to green after treatment also demonstrates the presence of Pb and MG in FB2.

The multifunctional treatment of *E. coli*, $Pb^{2+}$ and MG by FB is based on the synergistic effect of composition and specific structure: (1) the positive charge of FB favors electrostatic interactions, promoting *E. coli* attachment, altering cell permeability, and inducing cell membrane damage [52]; (2) the physical and/or mechanical disruption of the bacterial cell membrane by FB's special two dimensional flake structure and the oxidation sterilization from $Fe_3O_4$ in FB [4] can cause the release of cellular components, the inaction of protein and DNA, and finally the cell's death, similar to magnetic graphene [15]; (3) the adsorbed MG can react with the cell's membrane and cellular components, resulting in improved chemical disinfection; (4) there are various phosphate groups and adsorbed bacteria on the surface of FB1 which contribute to removing $Pb^{2+}$ and MG through physical and chemical bonds [43]. Taking into consideration the easy magnetic separation of FB, FS, and FSB, these nano-composites are sustainable materials for the successive removal of *E. coli* and mixed cationic pollutants from water.

## 4. Conclusions

In this study, three types of magnetic iron oxide/phosphate nanocomposites (FB, FS, and FSB) were synthesized to sequentially remove bacteria and then a mixture ($Pb^{2+}$ and MG) from contaminated water. The *E. coli* loaded on the nanomaterials is beneficial to the subsequent simultaneous removal of $Pb^{2+}$ and MG due to the surface charge change of the nanocomposite, from positive to negative; in addition the presence of *E. coli* on the nanocomposite surfaces improves the removal of $Pb^{2+}$ and MG, since they can be removed even by pure bacteria. On the other hand, MG serves as a very useful disinfectant for the bacteria loaded on the nanocomposite. Therefore, successive removal of *E. coli* and a mixture of $Pb^{2+}$ and MG can generate synergistic effects, which lead to more effective and complete treatment of these three pollutants from water by the as-prepared nanocomposites.

## Acknowledgements

This work was supported by the National Natural Science Funds of China (No. 51402153), the Jiangsu Natural Science Funds of China (No. SBK2017020336), and the Fundamental Research Funds for the Central Universities (No. KYZ201747). This work was partly supported by the National Science Foundation and the U.S. Environmental Protection Agency under NSF-EF0830117.

## Appendix A. Supplementary data

Supplementary material related to this article can be found, in the online version, at doi:https://doi.org/10.1016/j.colsurfa.2019.123598.

## References

[1] S. Chella, P. Kollu, E. Komarala, S. Doshi, M. Saranya, S. Felix, R. Ramachandran, P. Saravanan, V.L. Koneru, V. Venugopal, S.K. Jeong, A.N. Grace, Solvothermal synthesis of $MnFe_2O_4$-graphene composite-investigation of its adsorption and antimicrobial properties, Appl. Surf. Sci. 327 (2015) 27–36.
[2] L.P. Lingamdinne, Y.-Y. Chang, J.-K. Yang, J. Singh, E.-H. Cho, M. Shiratani, J.R. Koduru, P. Attri, Biogenic reductive preparation of magnetic inverse spinel iron oxide nanoparticles for the adsorption removal of heavy metals, Chem. Eng. J. 307 (2017) 74–84.
[3] A. Maleki, Z. Hajizadeh, V. Sharifi, Z. Emdadi, A green, porous and eco-friendly magnetic geopolymer adsorbent for heavy metals removal from aqueous solutions, J. Clean. Prod. 215 (2019) 1233–1245.
[4] J. Song, F. Zhang, Y. Huang, A.A. Keller, X. Tang, W. Zhang, W. Jia, J. Santos, Highly efficient bacterial removal and disinfection by magnetic barium phosphate nanoflakes with embedded iron oxide nanoparticles, Environ. Sci. Nano 5 (2018) 1341–1349.
[5] F. Zhang, X. Tang, Y. Huang, A.A. Keller, J. Lan, Competitive removal of $Pb^{2+}$ and malachite green from water by magnetic phosphate nanocomposites, Water Res. 150 (2019) 442–451.
[6] S. Herrmann, L. De Matteis, J.M. de la Fuente, S.G. Mitchell, C. Streb, Removal of multiple contaminants from water by polyoxometalate supported ionic liquid phases (POM-SILPs), Angew Chemie-Int. Ed. 56 (2017) 1667–1670.
[7] L. Akhigbe, S. Ouki, D. Saroj, Disinfection and removal performance for Escherichia coli and heavy metals by silver-modified zeolite in a fixed bed column, Chem. Eng. J. 295 (2016) 92–98.
[8] M. Hassan, R. Abou-Zeid, E. Hassan, L. Berglund, Y. Aitomaki, K. Oksman, Membranes based on cellulose nanofibers and activated carbon for removal of Escherichia coli bacteria from water, Polymers (Basel) 9 (2017).
[9] F. Zhang, J. Lan, Z. Zhao, Y. Yang, R. Tan, W. Song, Removal of heavy metal ions from aqueous solution using $Fe_3O_4$-$SiO_2$-poly(1,2-diaminobenzene) core-shell submicron particles, J. Colloid Interface Sci. 387 (2012) 205–212.
[10] M. Roosta, M. Ghaedi, N. Shokri, A. Daneshfar, R. Sahraei, A. Asghari, Optimization of the combined ultrasonic assisted/adsorption method for the removal of malachite green by gold nanoparticles loaded on activated carbon: experimental design, Spectrochim. Acta Part A-Mol. Biomol. Spectrosc. 118 (2014) 55–65.
[11] L.P. Lingamdinne, J.R. Koduru, Y.-Y. Chang, R.R. Karri, Process optimization and adsorption modeling of Pb(II) on nickel ferrite-reduced graphene oxide nanocomposite, J. Mol. Liq. 250 (2018) 202–211.
[12] T. Zou, C. Wang, R. Tan, W. Song, Y. Cheng, Preparation of pompon-like ZnO-PANI heterostructure and its applications for the treatment of typical water pollutants under visible light, J. Hazard. Mater. 338 (2017) 276–286.
[13] S. Singh, K.C. Barick, D. Bahadur, $Fe_3O_4$ embedded ZnO nanocomposites for the removal of toxic metal ions, organic dyes and bacterial pathogens, J. Mater. Chem. A Mater. Energy Sustain. 1 (2013) 3325–3333.
[14] Y. Huang, A.N. Fulton, A.A. Keller, Simultaneous removal of PAHs and metal contaminants from water using magnetic nanoparticle adsorbents, Sci. Total Environ. 571 (2016) 1029–1036.
[15] G. Gonavelli, C.-C. Chang, Y.-C. Ling, Facile synthesis of smart magnetic graphene for safe drinking water: heavy metal removal and disinfection control, ACS Sustain. Chem. Eng. 1 (2013) 462–472.
[16] Y. Haldorai, D. Kharismadewi, D. Tuma, J.-J. Shim, Properties of chitosan/magnetite nanoparticles composites for efficient dye adsorption and antibacterial agent, Korean J. Chem. Eng. 32 (2015) 1688–1693.
[17] A. Hatamie, H. Parham, B. Zargar, Z. Heidari, Evaluating magnetic nano-ferrofluid as a novel coagulant for surface water treatment, J. Mol. Liq. 219 (2016) 694–702.
[18] S. Singh, K.C. Barick, D. Bahadur, Surface engineered magnetic nanoparticles for removal of toxic metal ions and bacterial pathogens, J. Hazard. Mater. 192 (2011) 1539–1547.
[19] V.K. Sharma, T.J. McDonald, H. Kim, V.K. Garg, Magnetic graphene-carbon nanotube iron nanocomposites as adsorbents and antibacterial agents for water purification, Adv. Colloid Interface Sci. 225 (2015) 229–240.
[20] S. Singh, D. Bahadur, Catalytic and antibacterial activity of Ag decorated magnetic core shell nanosphere, Colloids Surf. B Biointerfaces 133 (2015) 58–65.
[21] S. Ma, S. Zhan, Y. Jia, Q. Zhou, Highly efficient antibacterial and Pb(II) removal effects of Ag-$CoFe_2O_4$-GO nanocomposite, ACS Appl. Mater. Interfaces 7 (2015) 10576–10586.
[22] Suman, A. Kardam, M. Gera, V.K. Jain, A novel reusable nanocomposite for complete removal of dyes, heavy metals and microbial load from water based on nanocellulose and silver nano-embedded pebbles, Environ. Technol. 36 (2015) 706–714.
[23] S.K. Das, M.M.R. Khan, T. Parandhaman, F. Laffir, A.K. Guha, G. Sekarana, A.B. Mandal, Nano-silica fabricated with silver nanoparticles: antifouling adsorbent for efficient dye removal, effective water disinfection and biofouling control, Nanoscale 5 (2013) 5549–5560.
[24] Z. Markova, K.M. Siskova, J. Filip, J. Cuda, M. Kolar, K. Safarova, I. Medrik, R. Zboril, Air stable magnetic bimetallic Fe-Ag nanoparticles for advanced antimicrobial treatment and phosphorus removal, Environ. Sci. Technol. 47 (2013) 5285–5293.
[25] M.K. Joshi, H.R. Pant, N. Liao, J.H. Kim, H.J. Kim, C.H. Park, C.S. Kim, In-situ deposition of silver-iron oxide nanoparticles on the surface of fly ash for water purification, J. Colloid Interface Sci. 453 (2015) 159–168.
[26] Y. Jiang, J.L. Gong, G.M. Zeng, X.M. Ou, Y.N. Chang, C.H. Deng, J. Zhang, H.Y. Liu, S.Y. Huang, Magnetic chitosan-graphene oxide composite for anti-microbial and dye removal applications, Int. J. Biol. Macromol. 82 (2016) 702–710.

[27] F. Zhang, B. Ma, X. Jiang, Y. Ji, Dual function magnetic hydroxyapatite nanopowder for removal of malachite green and Congo red from aqueous solution, Powder Technol. 302 (2016) 207–214.
[28] F. Zhang, X. Yin, W. Zhang, Development of magnetic $Sr_5(PO_4)_3(OH)/Fe_3O_4$ nanorod for adsorption of Congo red from solution, J. Alloys. Compd. 657 (2016) 809–817.
[29] L. Cui, Y. Wang, L. Hu, L. Gao, B. Du, Q. Wei, Mechanism of Pb(II) and methylene blue adsorption onto magnetic carbonate hydroxyapatite/graphene oxide, RSC Adv. 5 (2015) 9759–9770.
[30] A. Maleki, H. Movahed, P. Ravaghi, T. Kari, Facile in situ synthesis and characterization of a novel PANI/$Fe_3O_4$/Ag nanocomposite and investigation of catalytic applications, RSC Adv. 6 (2016) 98777.
[31] B. Pant, M. Park, J.H. Lee, H.Y. Kim, S.J. Park, Novel magnetically separable silver-iron oxide nanoparticles decorated graphitic carbon nitride nano-sheets: a multifunctional photocatalyst via one-step hydrothermal process, J. Colloid Interface Sci. 496 (2017) 343–352.
[32] Y. Jin, F. Liu, C. Shan, M. Tong, Y. Hou, Efficient bacterial capture with amino acid modified magnetic nanoparticles, Water Res. 50 (2014) 124–134.
[33] Y. Jin, J. Deng, J. Liang, C. Shan, M. Tong, Efficient bacteria capture and inactivation by cetyltrimethylammonium bromide modified magnetic nanoparticles, Colloids Surf. B Biointerfaces 136 (2015) 659–665.
[34] S. Zhan, Y. Yang, Z. Shen, J. Shan, Y. Li, S. Yang, D. Zhu, Efficient removal of pathogenic bacteria and viruses by multifunctional amine-modified magnetic nanoparticles, J. Hazard. Mater. 274 (2014) 115–123.
[35] S. Singh, K.C. Barick, D. Bahadur, Inactivation of bacterial pathogens under magnetic hyperthermia using $Fe_3O_4$-ZnO nanocomposite, Powder Technol. 269 (2015) 513–519.
[36] S. Zhan, D. Zhu, S. Ma, W. Yu, Y. Jia, Y. Li, H. Yu, Z. Shen, Highly efficient removal of pathogenic bacteria with magnetic graphene composite, ACS Appl. Mater. Interfaces 7 (2015) 4290–4298.
[37] J. Chen, B. Duncan, Z. Wang, L.-S. Wang, V.M. Rotello, S.R. Nugen, Bacteriophage-based nanoprobes for rapid bacteria separation, Nanoscale 7 (2015) 16230–1623.
[38] F. Halouane, R. Jijie, D. Meziane, C. Li, S.K. Singh, J. Bouckaert, J. Jurazek, S. Kurungot, A. Barras, M. Li, R. Boukherroub, S. Szunerits, Selective isolation and eradication of E. coli associated with urinary tract infections using anti-fimbrial modified magnetic reduced graphene oxide nanoheaters, J. Mater. Chem. B Mater. Biol. Med. 5 (2017) 8133–8142.
[39] J. Lin, M. Li, Y. Li, Q. Chen, A high gradient and strength bioseparator with nano-sized immunomagnetic particles for specific separation and efficient concentration of E-coli O157:H7, J. Magn. Magn. Mater. 378 (2015) 206–213.
[40] F. Nekouei, H. Noorizadeh, S. Nekouei, M. Asif, I. Tyagi, S. Agarwal, V.K. Gupta, Removal of malachite green from aqueous solutions by cuprous iodide-cupric oxide nano-composite loaded on activated carbon as a new sorbent for solid phase extraction: isotherm, kinetics and thermodynamic studies, J. Mol. Liq. 213 (2016) 360–368.
[41] L. Leng, X. Yuan, G. Zeng, J. Shao, X. Chen, Z. Wu, H. Wang, X. Peng, Surface characterization of rice husk bio-char produced by liquefaction and application for cationic dye (Malachite green) adsorption, Fuel 155 (2015) 77–85.
[42] D. Husaain, M. Najam-ul-Haq, A. Saeed, F. Jabeen, M. Athar, M.N. Ashiq, Synthesis of poly GMA/DVB and its application for the removal of Malachite Green from aqueous medium by adsorption process, Desalin. Water Treat. 53 (2015) 2518–2528.
[43] F. Zhang, Z. Zhao, R. Tan, W. Xu, G. Jiang, W. Song, Efficient and selective immobilization of $Pb^{2+}$ in highly acidic wastewater using strontium hydroxyapatite nanorods, Chem. Eng. J. 203 (2012) 110–114.
[44] F. Zhang, X. Chen, W. Zhang, Y. Ji, Dual-functionalized strontium phosphate hybrid nanopowder for effective removal of $Pb^{2+}$ and malachite green from aqueous solution, Powder Technol. 318 (2017) 128–134.
[45] L. Wang, J. Li, Q. Jiang, L. Zhao, Water-soluble $Fe_3O_4$ nanoparticles with high solubility for removal of heavy-metal ions from waste water, Dalton Trans. 41 (2012) 4544.
[46] J.M. Legal, M. Manfait, T. Theophanides, Applications of FTIR spectroscopy in structural studies of cells and bacteria, J. Mol. Struct. 242 (1991) 397–407.
[47] K.P. Tank, K.S. Chudasama, V.S. Thaker, M.J. Joshi, Cobalt-doped nanohydroxyapatite: synthesis, characterization, antimicrobial and hemolytic studies, J. Nanopart. Res. 15 (2013).
[48] J.J. Ojeda, M.E. Romero-Gonzalez, R.T. Bachmann, R.G.J. Edyvean, S.A. Banwart, Characterization of the cell surface and cell wall chemistry of drinking water bacteria by combining XPS, FTIR spectroscopy, modeling, and potentiometric titrations, Langmuir 24 (2008) 4032–4040.
[49] Y. Hu, H. Kazemian, S. Rohani, Y. Huang, Y. Song, In situ high pressure study of ZIF-8 by FTIR spectroscopy, Chem. Commun. 47 (2011) 12694–12696.
[50] G.M.S. El-Bahy, FTIR and Raman spectroscopic study of Fenugreek (Trigonella foenum graecum L.) seeds, J. Appl. Spectrosc. 72 (2005) 111–116.
[51] S. Horvat, A. Jakas, E. Vass, J. Samu, M. Hollosi, CD and FTIR spectroscopic studies of Amadori compounds related to the opioid peptides, J. Chem. Soc. Trans. 2 (1997) 1523–1528.
[52] E.I. Rabea, M.E.T. Badawy, C.V. Stevens, G. Smagghe, W. Steurbaut, Chitosan as antimicrobial agent: applications and mode of action, Biomacromolecules 4 (2003) 1457–1465.